RESEARCH ARTICLE

American Journal of Botany

Botanical Society of America
leading scientists and educators since 1893

Scaling of phloem hydraulic resistance in stems and leaves of the understory angiosperm shrub *Illicium parviflorum*

Juan M. Losada[1,2,3] and N. Michele Holbrook[1,2]

Manuscript received 21 June 2018; revision accepted 5 December 2018.

[1] Department of Organismic and Evolutionary Biology, Harvard University, 16 Divinity Avenue, Cambridge, MA 02138, USA

[2] Arnold Arboretum of Harvard University, 1300 Centre St., Boston, MA 02130, USA

[3] Author for correspondence (e-mail: juan.losada.r@gmail.com)

Citation: Losada, J. M. and N. M. Holbrook. 2019. Scaling of phloem hydraulic resistance in stems and leaves of the understory angiosperm shrub *Illicium parviflorum*. *American Journal of Botany* 106(2): 244–259.

doi:10.1002/ajb2.1241

PREMISE OF THE STUDY: Recent studies in canopy-dominant trees revealed axial scaling of phloem structure. However, whether this pattern is found in woody plants of the understory, the environment of most angiosperms from the ANA grade (Amborellales-Nymphaeales-Austrobaileyales), is unknown.

METHODS: We used seedlings and adult plants of the understory tropical shrub *Illicium parviflorum*, a member of the lineage Austrobaileyales, to explore the anatomy and physiology of the phloem in their aerial parts, including changes through ontogeny.

KEY RESULTS: Adult plants maintain a similar proportion of phloem tissue across stem diameters, but larger conduit dimensions and number cause the hydraulic resistance of the phloem to decrease toward the base of the plant. Small sieve plate pores resulted in an overall higher sieve tube hydraulic resistance than has been reported in other woody angiosperms. Sieve elements increase in size from minor to major leaf veins, but were shorter and narrower in petioles. The low carbon assimilation rates of seedlings and mature plants contrasted with a 3-fold higher phloem sap velocity in seedlings, suggesting that phloem transport velocity is modulated through ontogeny.

CONCLUSIONS: The overall architecture of the phloem tissue in this understory angiosperm shrub scales in a manner consistent with taller trees that make up the forest canopy. Thus, the evolution of larger sieve plate pores in canopy-dominant trees may have played a key role in allowing woody angiosperms to extend beyond their understory origins.

KEY WORDS ANA grade angiosperms; hydraulic conductivity; hydraulic resistance; *Illicium parviflorum*; leaves; phloem; sieve tube element; vasculature; xylem.

The ecological context in which angiosperms evolved has been hotly debated in the last decades. This uncertainty is, in part, due to the apparent contradiction between the relative recent rise of angiosperms, measured in geological time (approximately 125 million years ago), and the rapid diversification that led to their ecological dominance (Feild et al., 2003a, 2004). The success of flowering plants correlates with the evolution of anatomical innovations that improved their physiological performance in different environmental scenarios, such as leaf reticulate venation and large xylem vessels (Zwieniecki and Boyce, 2014; Boyce and Lee, 2017). Woody lineages are particularly interesting due to their ecological relevance, but most anatomical studies have focused on xylem and the physiology of water transport toward the top of the trees (Gleason et al., 2016; Woodruff et al., 2016; Olson et al., 2018). In contrast, only a few recent studies have dealt with the implications of phloem scaling in canopy-dominant woody angiosperms (Savage et al., 2017). Even less is known about the anatomy and physiology of the phloem in woody plants adapted to shaded environments.

Woody members of the ANA grade (Amborellales, Nymphaeales, Austrobaileyales; successive sister groups to all other flowering plants) are adapted to shaded conditions. These lineages, particularly Austrobaileyales and the monotypic *Amborella*, are excellent candidates to understand the physiological properties of arborescent plants that live in conditions with limited light. Most studies of extant members from this grade focused on the xylem (Feild et al., 2003b, 2004; Feild and Arens, 2005, 2007; Barral et al., 2013). Anatomically, these lineages are characterized by a small vessel lumen fraction in the stems (Bailey and Nast, 1948; Carlquist, 1982; Carlquist and Schneider, 2002), leaves with thick cuticles and large stomata, as well as irregular leaf venation (Hickey and Doyle, 1977; Upchurch et al., 1984; Carpenter, 2005; Coiffard et al., 2006). Comparable studies of the anatomy and physiological properties of the phloem are lacking.

Low light conditions necessarily result in low rates of photosynthesis and thus impose a critical constraint of understory growth. Previously, in situ measurements of the maximum photosynthetic activity in woody angiosperms of the ANA grade revealed an association between low primary productivity and low xylem hydraulic performance (Feild et al., 2005). While the hydraulics of the xylem are coupled with the sugar loading of the phloem in the mesophyll (Hölttä et al., 2006; Liesche et al., 2011; Nikinmaa et al., 2013; Rockwell et al., 2018), the performance of the phloem in leaves is still poorly understood. With a recent exception (Carvalho et al., 2017a, 2018), detailed evaluations of phloem architecture in leaves with reticulate venation are lacking. The paucity is in part due to the challenging manipulations required to quantify the geometry of the sieve tubes in the tapering veins, as well as difficulties in evaluating the velocity of the sap inside the sieve tubes, typically measured using a fluorescent dye tracer (Jensen et al., 2011; Etxeberria et al., 2016) or radiolabeled compounds (Knoblauch et al., 2016). Thus far, phloem sap velocities in leaves of adult plants (including petioles) have only been measured in a handful of species (Jensen et al., 2011). In addition, much less work has been devoted to the study of the phloem in seedlings, with a single exception from the Cucurbitaceae (Savage et al., 2013). As a result, comparisons of phloem structure and function between seedlings and adult plants have been missing so far. This information is critical to better understand the developmental plasticity of phloem in woody plants, as well as a possible variation in its transport efficiency through their ontogeny.

The widely accepted mechanism of phloem transport is the differential osmotic gradient generated between sources and sinks (Münch, 1930; Thompson and Holbrook, 2003; Pickard, 2012; Knoblauch and Peters, 2017), but the validity of this hypothesis has only recently been tested in herbaceous vines (Knoblauch et al., 2016) and trees (Liesche et al., 2017; Savage et al., 2017). In canopy-dominant tree species, long-distance geometrical scaling of the sieve elements of the phloem is conserved, resulting in a reduced hydraulic resistance of phloem conduits toward the base of the tree (Savage et al., 2017). Yet, understanding the overall flow capacity of the phloem requires quantification of sieve tube numbers alongside vascular tapering (i.e., tree/shrub branching). Sieve tube quantification has only been explored at single points of the stems in a few trees (Lawton and Canny, 1970; Ghouse et al., 1976; Ghouse and Jamal, 1979; Khan et al., 1992; Pace et al., 2011), but never by comparing different stem diameters, essential to evaluate whole plant transport.

Pursuing these questions, we investigated the angiosperm shrub *Illicium parviflorum* to gain a better understanding of phloem structure and function in the aerial parts of plants adapted to understory environments and through their ontogeny. Despite a restricted distributional range in the tropics of America and Asia, Illiciaceae is the largest family within the order Austrobaileyales. The latter is one of the three lineages that compose the ANA grade of flowering plants, and the sister group to all other angiosperms except Nymphaeales and *Amborella* (Mathews and Donoghue, 1999; Parkinson et al., 1999; Qiu et al., 2000; Soltis et al., 1999, 2018). While almost nothing is known of the phloem in these lineages (Bailey and Nast, 1948), this information could bring insights into their growth patterns and ecological adaptations. Our results include a novel quantification of sieve tube element number per cross-sectional area of the stems and major veins of leaves and characterization of phloem architectural traits related to the hydraulic efficiency of carbohydrate transport.

MATERIALS AND METHODS

Plant materials and growth conditions

Mature plants of *Illicium parviflorum* were grown in plastic pots in the greenhouses of the Arnold Arboretum of Harvard University, using high porosity growing medium PRO-MIX (PremierTech Horticulture and Agriculture Group, Riviere-du-Loup, QC, Canada), at 25°C ± 2°C with 75% relative humidity (Fig. 1). Plants were watered to field capacity every morning. Three seeds per pot were sown, and first seedlings (with two cotyledons) were visible 4 months after sowing. They were repotted individually and grown for three more months until the emergence of the first true leaves (approximately 3 cm long), which were used for the measurements described below. Due to the understory habit of these plants and based on our previous observations, high sun exposure was avoided with a dark net between the greenhouse roof and the plants (average photosynthetic active radiation [PAR] 100 μmol m^{-2} s^{-1}).

Measurements of carbon assimilation

Gas exchange was measured in three exposed leaves from three branches oriented in all directions in each mature plant (n = 3 adult plants), as well as two leaves from each seedling (n = 3 seedlings). Measurements were done at three time points during the day (08:30, 12:30, and 16:30 hours), once per week during February and March 2017. We used a LI-COR 6400 (LI-COR, Lincoln, NE USA), with light source, configured to track ambient PAR at each measurement (average 100 μmol m^{-2} s^{-1}). The reference CO_2 was 400 μmol mol^{-1}, the average leaf temperature 20.0°C ± 0.16°C (±SD), and vapor pressure deficit 1.06 ± 0.06 kPa (±SD). Results of photosynthetic activity were evaluated with a two-way ANOVA, using time of the day (morning, midday, and afternoon), and the developmental stage of the plant (adults and seedlings), as independent factors ($P < 0.05$).

Sample preparation for stem anatomy

Due to the shrubby nature of mature *Illicium parviflorum* plants, lateral branches were divided into four stem diameter classes (see Fig. 1): <2 mm (primary growth or early secondary growth), 4–6 mm (green shoots with secondary growth), 9–11 mm (stems with bark), and >21 mm (main stem). The length of each branch segment was measured, and the number and area of the leaves per unit length evaluated (n = 30). To observe changes in the vascular tissues with increasing stem diameters, we cut 5–10 cm long stem sections from each diameter class and three different plants with clippers and kept them in 1× Tris-buffered saline (TBS); 50 μm thick cross sections were then cut with a Reichert-Jung Hn-40 sliding microtome (Vienna, Austria), immediately mounted onto glass slides, and stained with a solution of 0.1% w/v aniline blue in K_3PO_4 (Linskens and Esser, 1957), which stains callose of the sieve plates. Samples were observed with either a Zeiss Axiophot microscope with epifluorescence and an AxioCam 512 Color connected to the AxioVision software (Zeiss, Oberkoche, Germany), using the DAPI narrow filter band (excitation 365 nm, bandpass 12 nm; dichroic mirror FT 395 nm; barrier filter LP397 nm). Individual images of the stem cross sections (taken with 5×/0.15 Plan-Neofluar objective) were aligned and merged into a composite image to visualize and measure the areas of the whole stem with Photoshop software (Adobe Systems, Newton, MA, USA).

Evaluation of sieve tube geometry in stems

To evaluate the length and the radius of the sieve tube elements, we used a microscalpel to hand-section a second set of samples from the same stem diameters described above. Sections were mounted on slides and stained with a mixture of 0.1% w/v aniline blue in K_3PO_4 and 0.1% w/v calcofluor white in 10 mM CHES buffer with 100 mM KCl (pH 10), which stains the cellulose from the cell walls of the sieve tube elements. Fluorescence of callose in the longitudinally oriented sieve plates was used to quantify the number and area of the lateral sieve areas composing the compound sieve plates connecting the individual tubes with a 40× objective magnification.

For quantifying the number of sieve tube elements, a third set of samples (2, 4, 6 and 11 mm diameter) of about 0.5 cm thickness was collected and then fixed in 4% w/v acrolein (Polysciences, Warrington, PA, USA) in a modified piperazine-*N*,*N*′-bis (2-ethanesulfonic acid) (PIPES) buffer adjusted to pH 6.8 (50 mM PIPES and 1 mM $MgSO_4$ from BDH, London, UK; and 5 mM EGTA) for 24 h, then rinsed thrice in the same buffer, and finally dehydrated through a series of increasing ethanol concentrations (10%, 30%, 50%, 70%, 80%, and 100%), 1 h each. Samples were incubated in the catalyzed solution of the resin Technovit 8100 (Electron Microscopy Sciences, Hatfield, PA, USA) for at least 3 months, and finally embedded under anoxic conditions and at 4°C. Later, blocks were mounted on microtome studs and serially sectioned at 4 µm with a Leica RM2155 rotary Microtome (Leica Microsystems, Wetzlar, Germany). After mounting them on Superfrost slides, they were stained with aniline blue and calcofluor as described previously to quantify both the number of sieve tube elements (the conducting cells of the phloem) compared to the total axial elements of the phloem between the ray parenchyma, which is an integral constituent of the phloem, but served as a topographical reference for cell quantifications in sections.

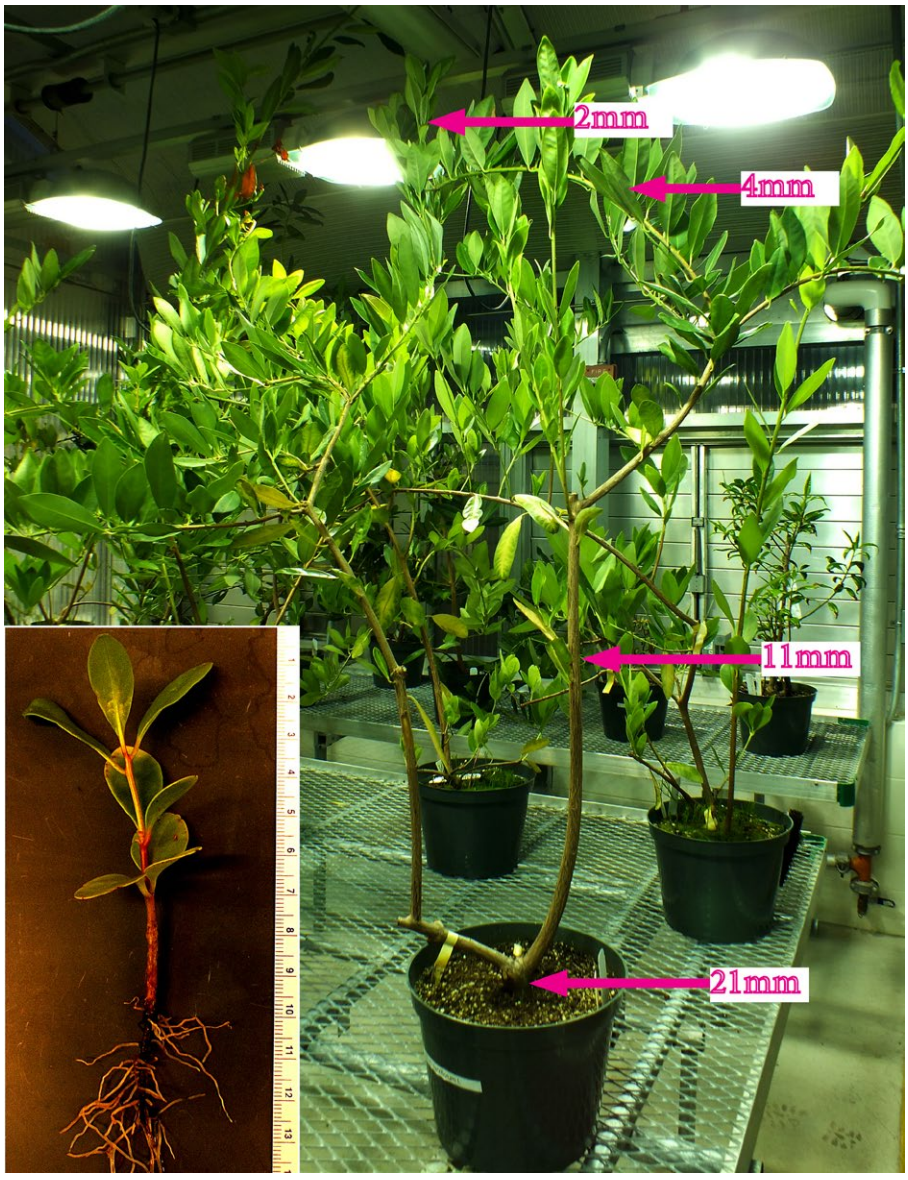

FIGURE 1. *Illicium parviflorum* shrubs in the greenhouse. Arrows indicate the diameter of the stem where samples were obtained. Distal parts correspond with thinner stems and areas of primary growth. Inset shows an image of an uprooted seedling. Scale in centimeters.

All samples were imaged with a Zeiss LSM700 Confocal Microscope (20×/0.8 M27 Plan-Apochromat objective for cross sections and 63×/1.40 Oil DIC M27 Plan-Apochromat objective for longitudinal sections) using the 405 nm laser band to excite the sample and a Zen Black 2010 software connected to a Zeiss HR camera to create the final compound tiles. Serial tile images obtained from resin sections were aligned with Photoshop software, then the axial cells of the phloem between ray parenchyma and the sieve tube elements were quantified (Appendix S1). To estimate the total number of sieve tubes per stem diameter, we calculated the tube number per these areas that are between the phloem parenchyma rays and multiplied that number by the estimated total phloem area at each stem diameter. Note that this will slightly overestimate the number of sieve tubes, given that the area of the uniseriate phloem ray parenchyma was not subtracted from the estimate of total phloem area.

Evaluation of pore size of sieve plates

To evaluate in detail the size of pores that make up the sieve plates, we cut another batch of wood sections, which were immediately frozen in liquid nitrogen, transferred to super-chilled ethanol, and then sectioned in the same orientation of the sieve plates at each diameter. After that, the cut sections were incubated within a mixture of 0.1% w/v proteinase K dissolved in 50 mM Tris-HCl buffer, 1.5 mM Ca^{2+} acetate and 8% Triton X-100, pH 8.0 (Mullendore

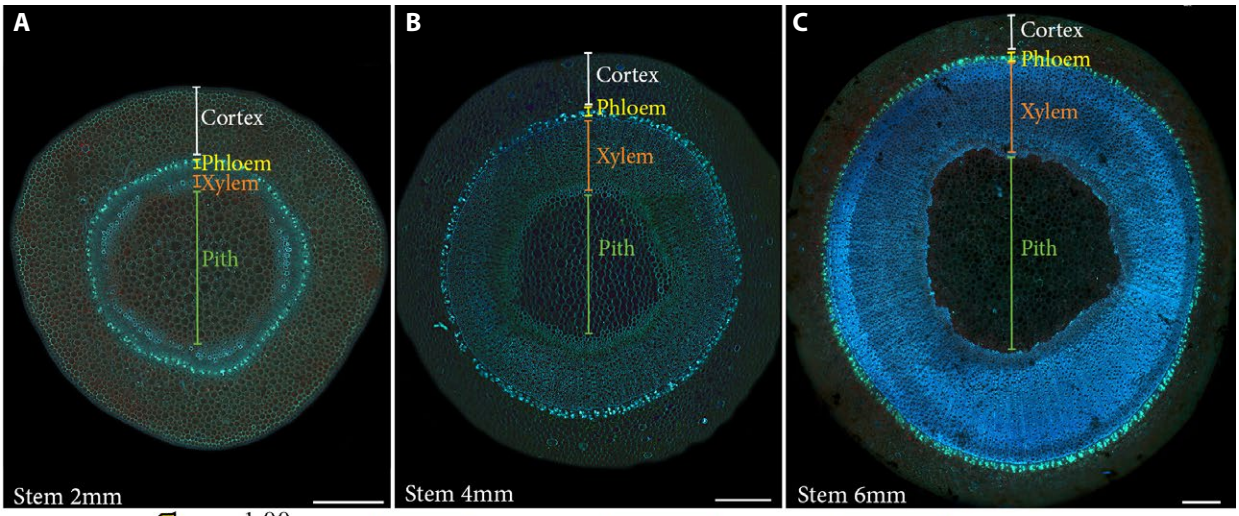
A
Cortex
Phloem
Xylem
Pith
Stem 2mm
B
Cortex
Phloem
Xylem
Pith
Stem 4mm
C
Cortex
Phloem
Xylem
Pith
Stem 6mm

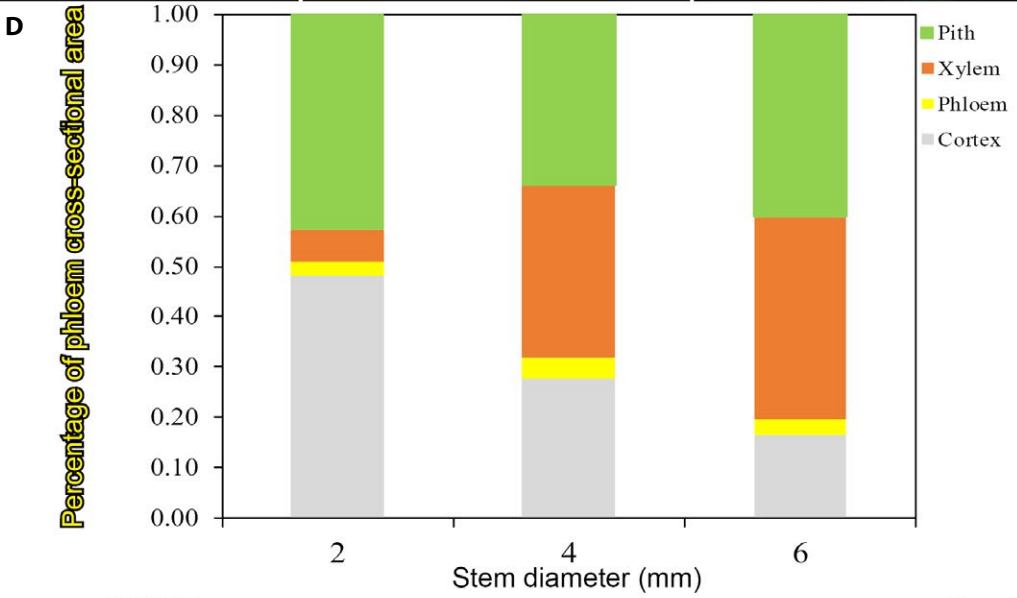
D
Percentage of phloem cross-sectional area
1.00
0.90
0.80
0.70
0.60
0.50
0.40
0.30
0.20
0.10
0.00
2
4
6
Stem diameter (mm)
Pith
Xylem
Phloem
Cortex

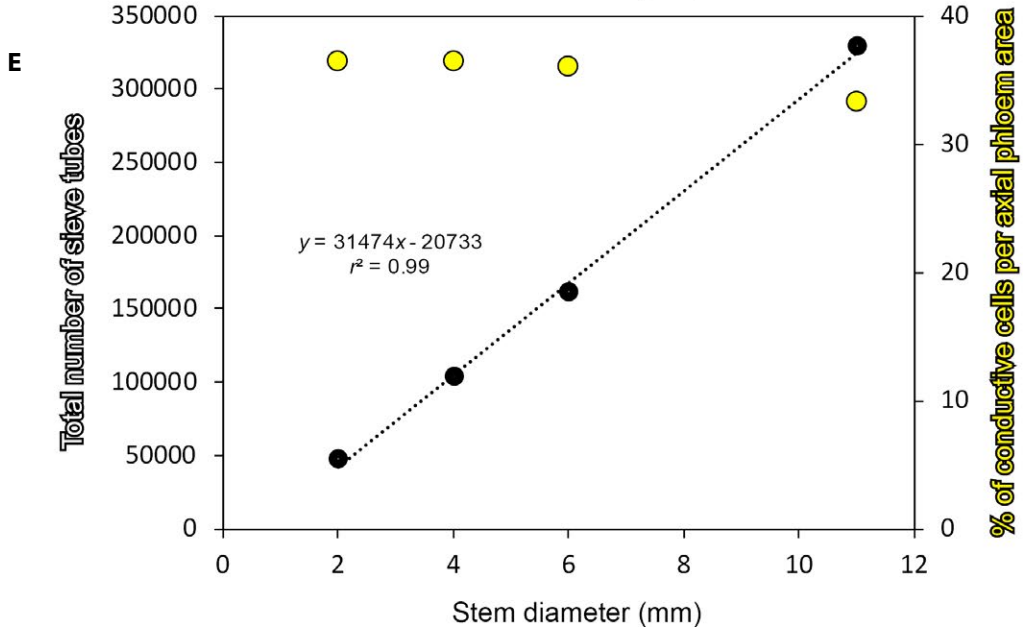
E
Total number of sieve tubes
350000
300000
250000
200000
150000
100000
50000
0
y = 31474x - 20733
r² = 0.99
0
2
4
6
8
10
12
Stem diameter (mm)
40
30
20
10
0
% of conductive cells per axial phloem area

FIGURE 2. Anatomy of stems in *Illicium parviflorum*. (A–C) Cross sections stained with aniline blue for callose. (A) Stem with early secondary growth, 2 mm diameter. (B) Stem with secondary growth, 4 mm diameter. (C) Stem showing bark, 6 mm diameter. (D) Percentage of cross-sectional areas occupied by the cortex and epidermis (grey, lower bar), phloem (yellow), xylem (orange), and pith (green, upper bar) tissues at different developmental stages of the stems based on their diameter. (E) Sieve tube element number per stem cross-sectional area: black solid circles represent the relationship between the total number of sieve tube elements and stem diameter; yellow open circles represent the percentage of sieve tubes (conductive area) in the axial areas that are between the phloem ray parenchyma. Scale bars = 500 μm.

et al., 2010), using a water bath at 60°C for 2 weeks. After rinsing with ethanol to deactivate the proteinase and washing them thrice with water, they were incubated with a 1% w/v aqueous solution of α-amylase for at least 2 days at 60°C, then rinsed thrice in water and finally freeze-dried for 24 h. Samples were then mounted on SEM studs and sputter-coated with gold-palladium using a Denton Vacuum Desk II Sputter Coater for 180 s at 20 V and 6.67 Pa. Studs with samples coated with gold-palladium were imaged with a JEOL-6010LV scanning electron microscopy (SEM) (JEOL, Peabody, MA, USA) using high vacuum and an accelerating voltage of 10–15 kV. Pore size was evaluated in at least 10 samples (n = 140 pores) of the largest stem diameters (11 mm and 21 mm). Note that we used this technique to evaluate pore size because it was previously demonstrated that it avoids artifacts such as sieve tube collapse and offers the most accurate measures of pore size resembling the in vivo condition.

Sample preparation for leaf anatomy

Transverse serial sections of the petiole, midrib, and secondary veins of mature *I. parviflorum* leaves were hand-cut, stained with aniline blue and calcofluor, and imaged with a confocal microscope (details below). For examining changes in the area of the xylem, phloem, and sclerenchyma along the major vein of mature leaves, three sequential cross sections of the petiole, midrib and tip of the major vein were obtained from five mature leaves, then imaged and manually outlined with the Image J 1.51d software (National Institutes of Health, Bethesda, MD, USA; Appendix S2). Longitudinal sections of the same vein areas from the petiole, the midrib, and second and third order veins were obtained from five different leaves and imaged with the protocol described below for quantification of length and radius of the sieve tube elements.

Due to the small size of leaves from seedlings, leaf material was fixed in 4% acrolein, then embedded in Technovit 8100 before serial sectioning with a microtome as previously described. Variation among areas, sieve tube lengths, radius, and numbers from leaves were averaged and means compared among the different vein orders using a one-way ANOVA and Tukey's honestly significant difference test at a $P < 0.05$. All statistical analyses were performed with SPSS version 24 (IBM, Armonk, NY, USA).

Measurements of phloem sap velocity

Phloem transport velocity was measured by tracking the movement of the fluorescent dye carboxifluorescein (CF) (reviewed by Knoblauch et al., 2015) in the secondary veins of living mature plants and seedlings at 11:00 hours each day. After saturating the soil with water, and taking advantage of the flexibility of the branches from shrubs, we took three mature plants and nine seedlings to the laboratory, and the leaves were immobilized on the microscope stage with the abaxial surface exposed upward, avoiding petiole twisting, which might affect sap flow within the phloem. A 10 μL droplet of a mixture containing 0.01 M CF diacetate in 1:10 mixture of acetone and distilled, deionized water, supplemented with 0.1% of the surfactant SilEnergy (RedRiver Specialties, Shreveport, LA, USA) was applied with a micropipette to the distalmost part of the secondary veins (adapted from Jensen et al., 2011; Savage et al., 2013). To allow better permeabilization of the dye, we used the tip of the pipette to slightly abrade the thick cuticle, and the small window opened (approximately 1 mm^2) was covered with the liquid during the experiment to prevent desiccation. To track the movement of the dye, we used a portable Stereo Microscope Fluorescence Adapter with 510–540 nm excitation wavelength, and a long pass 600 nm filter band (NIGHTSEA, Lexington, MA, USA). Time-lapse images were obtained every 10 s for 20 to 40 min with a Zeiss v12 dissecting microscope using the 0.63× PlanApo objective and an AxioCam 512 Color camera connected to the AxioVision software. Velocity was calculated by tracking the time taken by the dye front to travel a known distance.

RESULTS

Anatomy of the stems in *Illicium parviflorum*

Illicium parviflorum shrubs have numerous lateral branches and a short thicker stem (Fig. 1). Younger branches are green (2–10 mm diameter) and support spirally arranged leaves, whereas older branches (>10 mm diameter) have visible bark and seldom retain leaves. The length of the branches scales proportionally with their diameter, and thus the stems with 2 mm diameter reach up to 10 cm long, whereas 6–10 mm diameter stems extend through 50 cm. While the ratio of leaf number to stem length is higher in the youngest stems (0.7 ± 0.07 SE) compared with older ones (0.5 ± 0.03 SE), the average leaf area increases from 13.4 cm^2 in thinner stems (2 mm diameter, primary growth) to 20.7 cm^2 in older ones (6 mm diameter). Given the width–length relationship, we considered the diameter of the stem as a useful reference to evaluate apical to basal transport in the plant.

To understand the area that each tissue occupies in the cross section of the stems, we measured the radius of the ring formed by the cortex, the phloem, the xylem, and the pith, and calculated the area as $A = \pi(R^2 - R_n^2)$, where R_n is the radius of each ring tissue, and R the total radius of the stem. We then normalized these areas to the percentage of total cross-sectional area occupied, which revealed that the cross-sectional area of the cortical tissue (including the epidermis) decreased as the stem diameter increased (Fig. 2A–C) and the opposite pattern for the xylem tissue. Strikingly, the proportion of the cross-sectional area occupied by the phloem tissue was maintained in all stem diameters evaluated (Fig. 2D). Because the phloem axial elements can easily be identified between the phloem ray parenchyma, we quantified the proportion of sieve tubes per area between the phloem ray parenchyma in different stem diameters to estimate the total number of tubes (Appendix S1). The

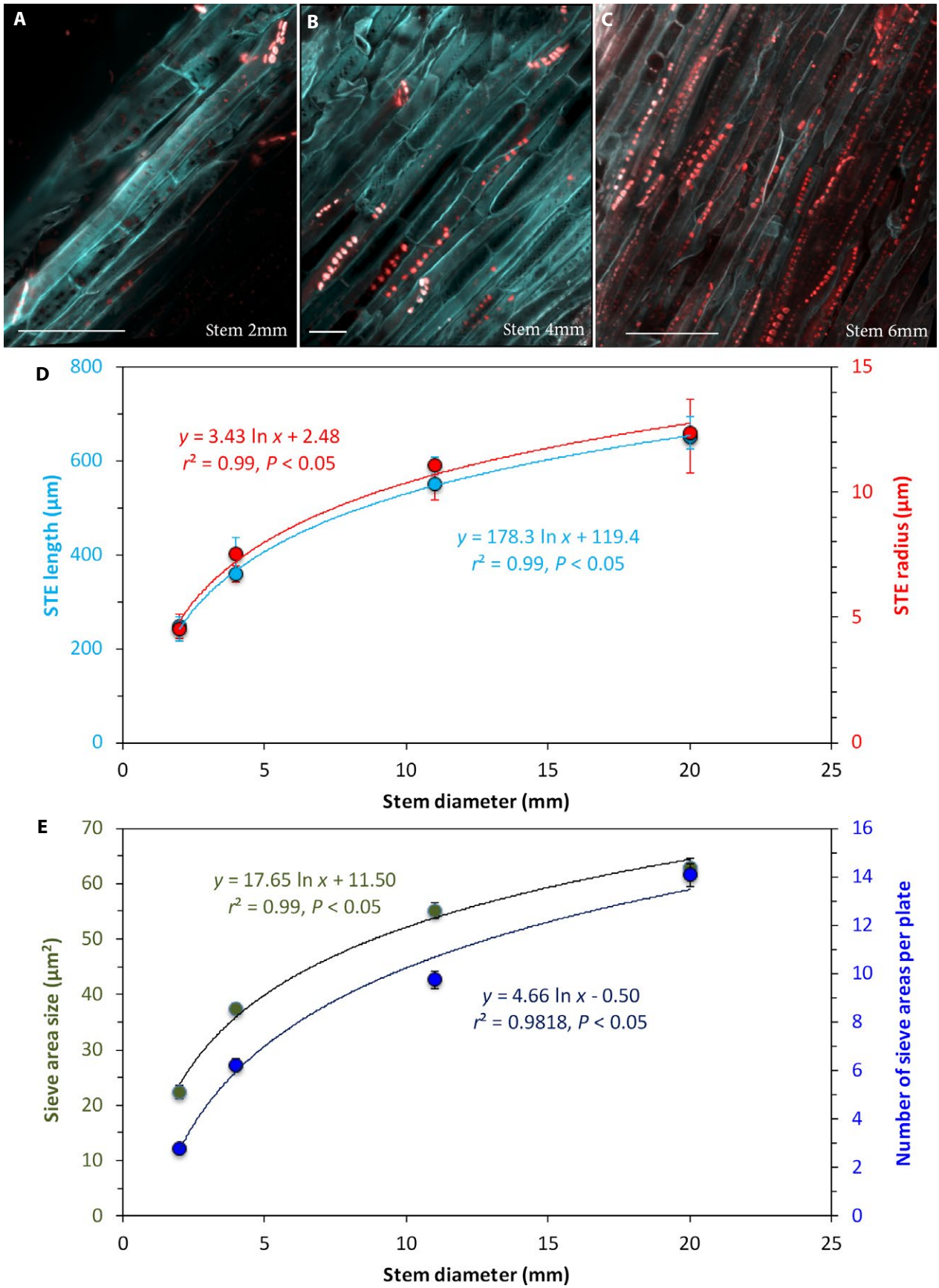
A
Stem 2mm
B
Stem 4mm
C
Stem 6mm
D
y = 3.43 ln x + 2.48
r² = 0.99, P < 0.05
y = 178.3 ln x + 119.4
r² = 0.99, P < 0.05
STE length (µm)
STE radius (µm)
Stem diameter (mm)
E
y = 17.65 ln x + 11.50
r² = 0.99, P < 0.05
y = 4.66 ln x - 0.50
r² = 0.9818, P < 0.05
Sieve area size (µm²)
Number of sieve areas per plate
Stem diameter (mm)

FIGURE 3. Phloem in stems of *Illicium parviflorum*. (A–C) Longitudinal sections of the stems stained with aniline blue for callose and calcofluor white for cellulose. (A) Sieve tube element in a stem with early secondary growth (2 mm diameter) showing cell walls in cyan and sieve plates in red. (B) Sieve tube elements in 4 mm diameter stem. (C) Sieve tube element network in 6 mm diameter stem. (D) Geometric relationships between sieve tube element (STE) length (light blue), radius (red), and diameter of the stem. (E) Relationship between number of sieve areas per end plate (dark blue, lower line) and their size (green, upper line) across stem diameters. Logarithmic regression curves at $P < 0.05$; bars display standard error (SE). Scale bars: A = 100 µm; B = 200 µm; C = 500 µm.

proportion of conductive cells (number of sieve tubes/total number of phloem cells in each axial area) was maintained at approximately 30% in all of the stem diameters evaluated, while the estimated total number of sieve tubes increased linearly with stem diameter (r^2 = 0.99; $P < 0.05$; Fig. 2E).

The morphology of individual sieve tube elements varied across stem diameters, with the number of sieve areas per plate connections between tubes increasing as stem diameters increased (Fig. 3A–C). The length (l) and radius (r) of individual sieve tube elements showed a logarithmic positive relationship with stem diameter ($P < 0.05$; Fig. 3D). Similarly, both the area and number of sieve plates followed a positive logarithmic relationship with stem diameter ($P < 0.05$; Fig. 3E). The average radius of sieve plate pores in the two large stem diameter classes was 0.22 µm ± 0.005 SE. We were unable to quantify the pore size of smaller diameter stems because the sieve pores were occluded with an amorphous material.

Leaf vascular anatomy in *Illicium parviflorum*

The mature leaves of *I. parviflorum* have reticulate venation (Fig. 4A). Veins extend from the small petiole (1 cm long on average), through the midrib to fourth order veins, with higher vein orders difficult to disentangle. Cross sections of the major veins in leaves from adult plants revealed that both the phloem and the xylem comprise three cell types: conduits, axial parenchyma, and ray parenchyma (Fig. 4B, E; Appendix S1), similar to the organization observed in the stem vasculature. A sheath of thick-walled pericyclic fibers surrounds the vasculature of the primary and higher order veins in the leaf lamina (Fig. 4C, D), which is largely absent in the petiole. The total area occupied by the vascular tissues from the petiole toward the tip of the midrib declines (Appendix S2), but the number of conducting elements of the phloem and xylem located in the areas between ray parenchyma (taken as a reference for quantifications), as well as their respective lumen areas, is maintained along the entire midrib (Appendix S3). These results suggest that the decline in the conductive areas of the major vein toward the midrib tip is due solely to the gradual reduction of the number of phloem–xylem areas between ray parenchyma. Each area between ray parenchyma maintains the 1:1 xylem–phloem cell number in the secondary veins, although their number and lumen size are reduced by almost an order of magnitude compared with the major vein (Fig. 4E). Leaf vasculature is markedly different in seedlings, where the xylem and phloem cells are still differentiating. Between them, several rows of square and thin-walled cells likely correspond with cambial tissue (Fig. 4F–H; Appendix S4).

Quantifications of the length and radius of sieve tube elements in leaves of *Illicium parviflorum* reveals that both dimensions decrease from the major vein to the higher order veins (Fig. 5A), yet are conserved between the midrib and the petiole (Fig. 5A, B). Unfortunately, quantifying the length and radius of the sieve tube elements in fourth vein orders was impossible due to the massive presence of sieve areas along their lateral cell walls (Fig. 5C). Strikingly, the sieve tube elements of the leaves from seedlings were longer and wider compared with mature leaves (Fig. 5D, E).

Assimilation rates and phloem sap velocity

Neither photosynthetic activity between adult plants and seedlings of *Illicium parviflorum*, nor the interaction between developmental stage and time of measurement, was significant (two way ANOVA; $r^2 = 0.71$; $P = 0.11$, $P = 0.28$, respectively). Maximum rates of 4–5 µmol CO_2 m^{-2} s^{-1} were observed at midday (Fig. 6). To evaluate the velocity of transport through the phloem, we monitored the fluorescence front of a dye tracer along the secondary veins of both adult plants and seedlings (Fig. 7). While this velocity was very low for adult plants, 4.94 ± 1.10 SE µm s^{-1} ($n = 3$) (compared with other angiosperm species), the veins of seedlings exhibited a velocity that was nearly three times higher, 14.44 ± 1.70 SE µm s^{-1} ($n = 5$), pointing to a regulation of sap flow velocity through the phloem in *I. parviflorum* plants depending on their developmental stage.

Sieve tube hydraulic resistance in stems and leaves

From the collected anatomical data, we computed the hydraulic resistance of sieve tubes from thinner and shorter branches, which have the smallest tubes, to the stems at the base of the shrub, which exhibit the widest diameters and larger sieve tubes. Sieve tube resistance can be expressed as $R_{tube} = R_{lumen} + R_{plate}$. Lumen resistance depends on both the geometry of the tubes themselves and the viscosity of the sap flowing within, which we assume here as η = 1.7 mPa, an estimate obtained from previous measurements (Knoblauch et al., 2016). R_{plate} is determined by the number and size of sieve pores (Jensen et al., 2012a, b), with pore radius the most influential variable affecting resistance (see also Jensen et al., 2014; Savage et al., 2017). Note that because we were unable to measure the pore diameters of the smaller stems, for our calculations we assume that pore size does not vary.

Sieve tube hydraulic resistance per length in *I. parviflorum* has an inverse relationship with the diameter of the stems (Fig. 8A), but the magnitude of this decrease is modest compared to patterns recently reported for trees (Savage et al., 2017). The slight decrease is because of the scaling dimensions of the sieve tubes (longer and wider toward the base of the shrub), but also the increasing number of sieve areas—and thus the number of pores—in larger diameter branches. To understand the influence of this decreasing resistance on the pressure required to drive sap flow in the leaves, we used the resistor analogy recently applied to trees (Savage et al., 2017). This model assumes that the differential pressure (Δp) across transport length L is proportional to the hydraulic resistance per length of sieve tubes, R (Pa s m^{-4}) and the sap flow rate Q (m^3 s^{-1}) expressed as $\Delta p/L = QR$. We calculated Δp across a transport length (L) for different diameter stems, assuming a constant linear flow velocity (U), and the average sieve element radius (r) and length (l), and our estimate of sieve tube resistance R_{tube} (Pa s m^{-3}):

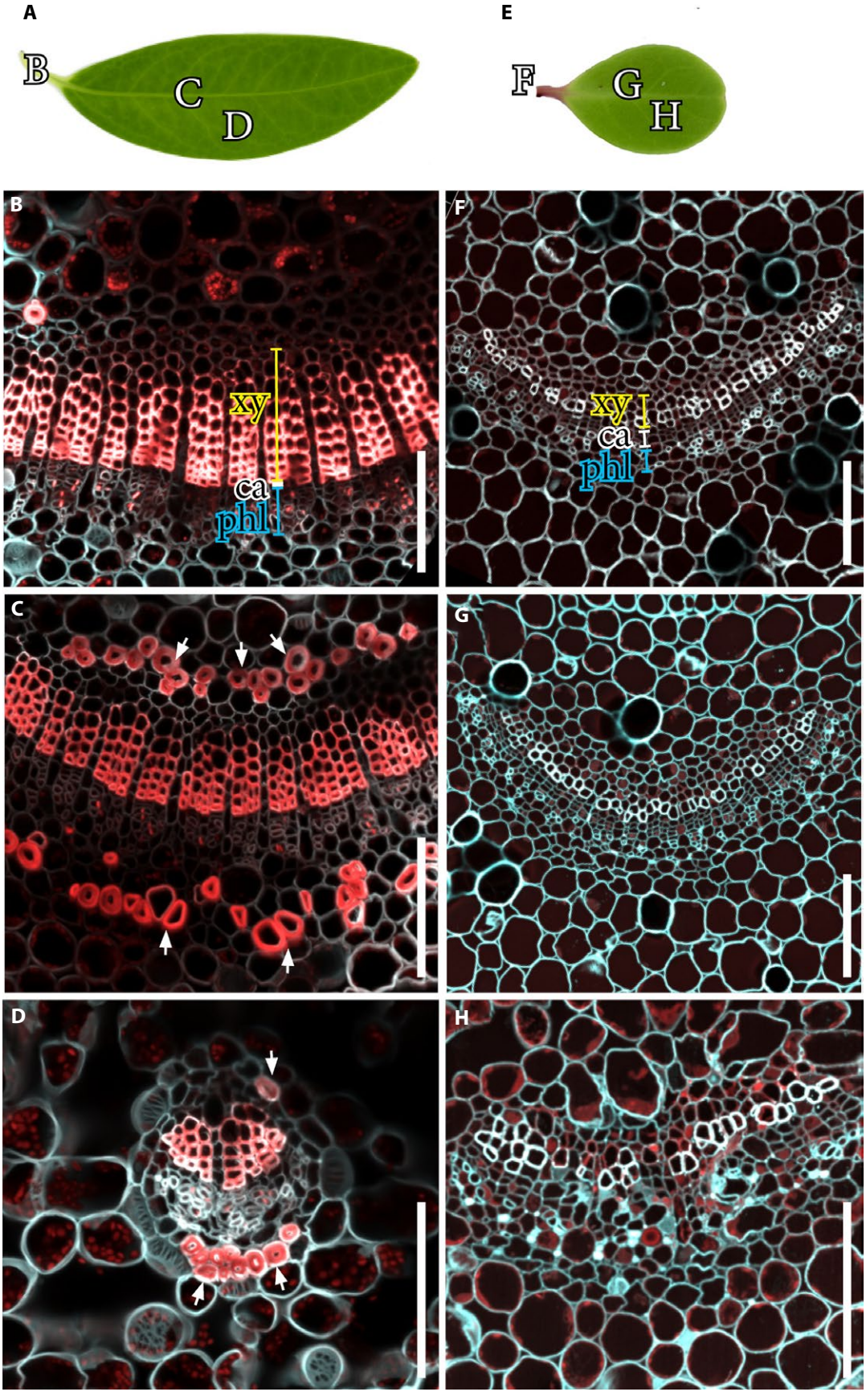
A
B
C
D
E
F
G
H
xy
ca
phl
xy
ca
phl

FIGURE 4. Anatomy of leaves in *Illicium parviflorum*. (A) Mature leaf showing adaxial surface and reticulate venation. (B) Vasculature of petiole showing arrangement of xylem (Xy), cambium (Ca), and phloem (Phl). (C) Cross section of the midrib showing a similar organization but surrounded by a pericyclic fiber cap (white arrows). (D) Secondary vein showing reduced xylem and phloem tissue compared with the primary vein. (E) Leaf of seedling. (F) Petiole showing differentiating xylem (yellow), several rows of cambial cells (white), and differentiating phloem (blue) tissues. (G) Similar organization in the midrib. (H) Secondary vein. (B–D, F–H) Cross sections stained with aniline and calcofluor white. ca, cambium; phl, phloem; xy, xylem. Scale bars: 500 μm.

$$\Delta p = \frac{\pi r^2 ULR_{\text{tube}}}{l}$$

Assuming the phloem sap velocity measured in mature plants (5 μm s^{-1}), the differential pressure required to transport sap in a 1-m long branch is very low (0.05 MPa for the smallest branch diameters). Thus, with a fixed viscosity and relatively low pressures, the small branches of *Illicium parviflorum* could be much longer without compromising carbohydrate transport. The higher phloem sap velocity measured in seedlings implies that the pressure required to transport the same distance would increase, yet the estimated pressure difference (0.16 MPa) is within the range of most measured angiosperms. It has to be noted that seedlings, similar to younger branches, rarely reach lengths longer than 0.05 m without widening their stems.

Using the geometric variables of the sieve tube elements from leaves, we evaluated the lumen hydraulic resistance in different vein orders (Fig. 8B). Note that lumen resistance is one of the two components of the tube resistance because we would need to measure the pore size in the sieve plates of different vein orders in the leaves, which was not possible in this study, and we note that pore size measurements in the sieve plates of angiosperm leaves are extremely rare. However, for comparative purposes, the R_{lumen} of the small branches is 1.6×10^{14} Pa s m^{-3}, a similar value to that of the petioles (1.0×10^{14} Pa s m^{-3}). As in the stems, phloem hydraulic resistance decreased by over an order of magnitude from tertiary veins to the petiole.

DISCUSSION

Scaling of phloem geometry in the stems of *Illicium parviflorum*

The current work shows that the increase in stem diameter in *I. parviflorum* toward the base of the shrub correlates with a developmental scaling of sieve tube structure. Comparable values of length and width of the sieve tubes have been only recently reported in angiosperm trees, pointing to a conserved mechanism associated with attainment of an arborescent growth form (Liesche et al., 2017; Savage et al., 2017). However, pore sizes of the sieve plates were substantially smaller in *Illicium* (in average, the radius is 0.22 μm for wider branches, within the lowest range reported for angiosperm trees). Sieve plate pore radius has been estimated as the most influential variable affecting sap flow resistance within sieve tube (Esau et al., 1962; Mullendore et al., 2010; Jensen et al., 2012a, b; Savage et al., 2017). In *Illicium*, even assuming that the pore diameters of stems with smaller girths are equal to our measured pores, phloem hydraulic resistance decreases toward the base of the shrubs. Should pore radius be reduced in smaller branches, following a similar pattern to that previously observed in trees (Savage et al., 2017), those differences will be even greater. If small pore size holds true for other angiosperms of the ANA grade, tiny pores could be an ancestral feature of woody flowering plants and would also be consistent with the high xylem resistance previously reported in the wood of these extant lineages (Feild et al., 2003a, 2004, 2009). Remarkably, the proportional cross-sectional area of the phloem in different stem diameters of *I. parviflorum* is conserved, contrasting with a reduction of cortical tissue and an increase in xylem tissue.

The scaling of lumen diameter and number of xylem elements toward the base of woody angiosperms have been widely studied (Hölttä et al., 2006, 2009, 2013; Sevanto et al., 2011; Petit and Crivellaro, 2014; Diaz-Espejo and Hernandez-Santana, 2017) because quantification of vessels in cross section is straightforward, whereas counting the sieve tube elements is more challenging. Due to the paired structure–function relationship between the phloem and the xylem (reviewed by Savage et al., 2016; Seleznyova and Hanan, 2018), understanding hydraulic transport in woody organisms requires a better understanding of sieve tube numbers along the plant, so far missing in woody lineages. Indeed, some reports in speciose tribes such as the Bignonieae (Bignoniaceae) have shown great variability in the morphological properties of phloem elements and suggested a high functional specialization of the sieve tube elements in the secondary phloem (Pace et al., 2011, 2015). In most studies, sieve tube number estimations were based on single point measurements in the stems, such as the 2/3 sieve tube proportion (number of sieve tubes relative to total phloem cells) inferred by Münch (1930), which was later challenged by quantifications of sieve tubes in the stems of other angiosperm trees, such as the 12–26% in six *Cassia* species (Ghouse and Jamal, 1979), 17–35% in members of the Myrtaceae (Ghouse et al., 1976), 54–74% in *Sterculia tragantha* and *Bombax bounopozense* (Lawton and Canny, 1970), or 11–59% in leguminous trees (Khan et al., 1992). Similarly, numbers can vary depending on whether the phloem is regular or variant type, as found in certain families such as Bignoniaceae, where regular sieve tube elements may occupy 7% of the total phloem area, whereas variant sieve tube elements reach 34% of the total phloem area (Pace et al., 2011).

Yet, these single point measurements offer only a partial picture (see also Canny, 1973). Here we used serial sections to estimate the total number of sieve tubes per cross-sectional area of the stem at different positions along the plant. While the proportion of conductive elements per phloem areas between ray parenchyma (30%) is maintained in all stem diameters in *Illicium parviflorum*, consistent with the similar proportion of vessels in the xylem (Feild et al., 2003a), the total number of conductive tubes increases linearly with stem diameter. In stems with early secondary growth, the average leaf area supplying photosynthates doubles from thinner to thicker stems and the estimated number of sieve tubes follows a similar trend. The lack of sieve tube number quantification across different stem diameters in the majority of woody angiosperms hampers a comparative

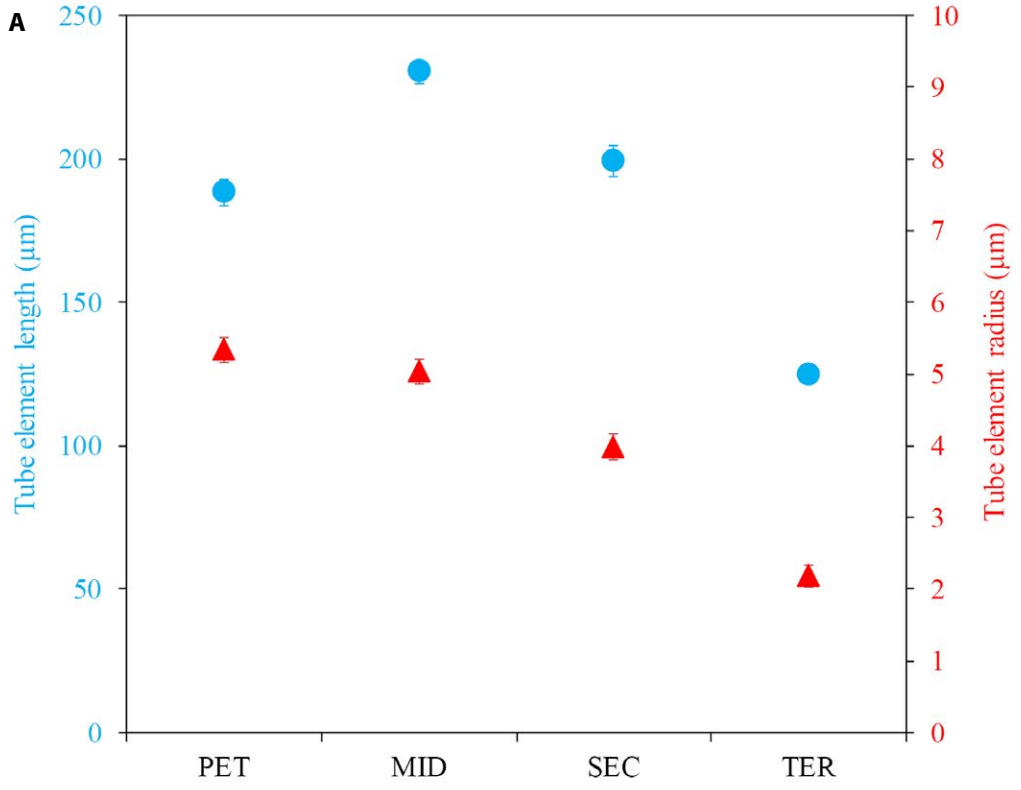
A
Tube element length (µm)
Tube element radius (µm)
250
200
150
100
50
0
10
9
8
7
6
5
4
3
2
1
0
PET
MID
SEC
TER

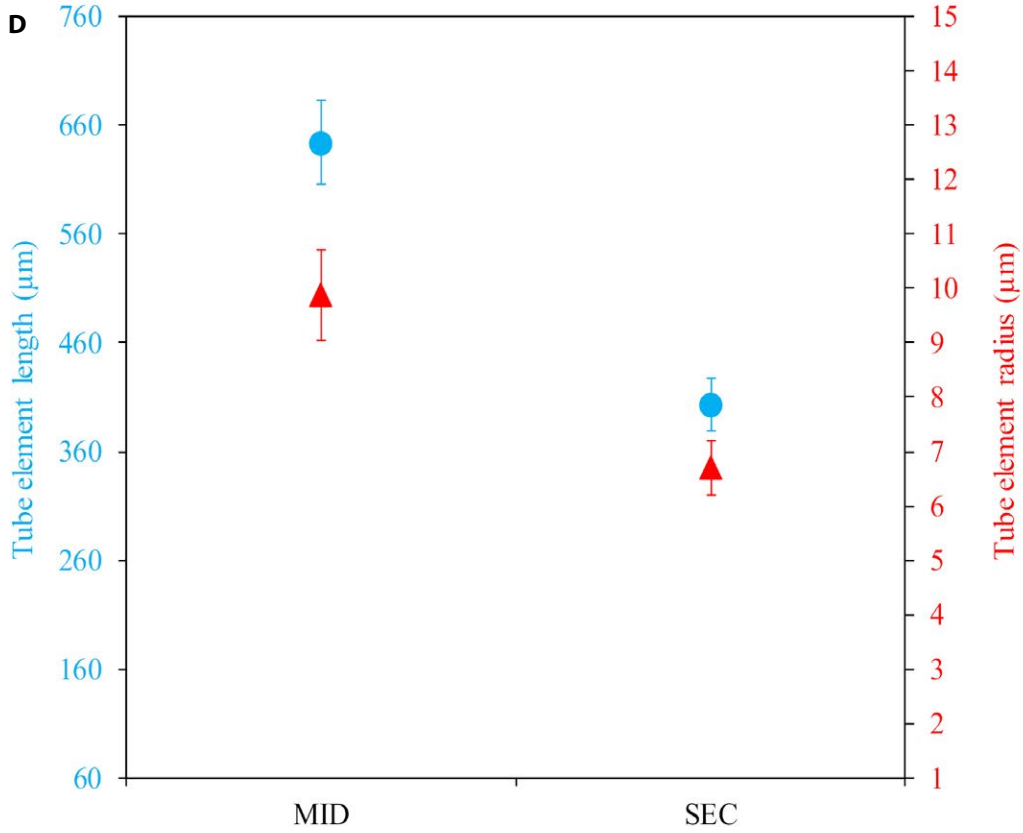
D
Tube element length (µm)
Tube element radius (µm)
760
660
560
460
360
260
160
60
15
14
13
12
11
10
9
8
7
6
5
4
3
2
1
MID
SEC

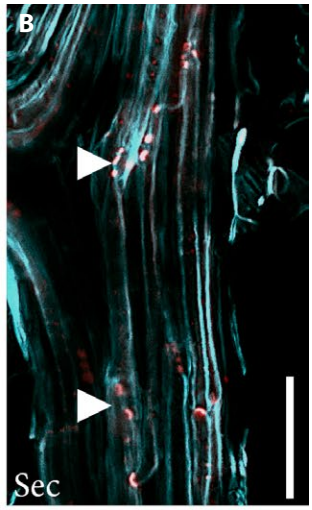
B
Sec

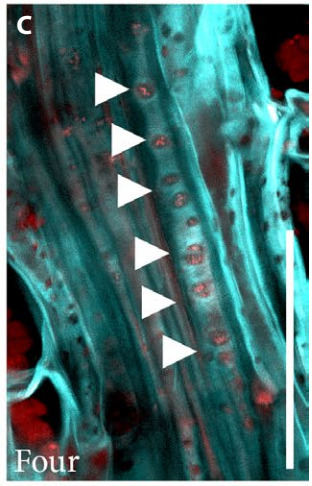
C
Four

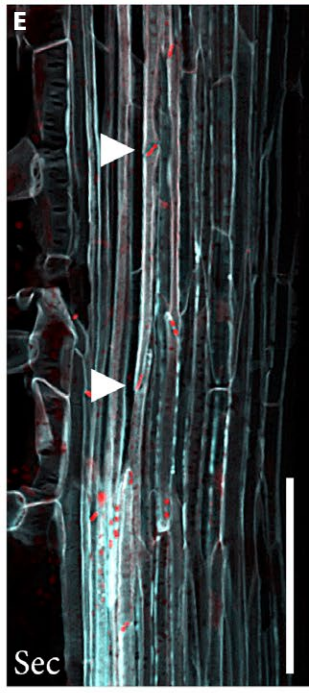
E
Sec

FIGURE 5. Phloem in leaves of *Illicium parviflorum*. (A) Scaling relationship between sieve tube element length (blue circles) and radius (red triangles) across major veins in mature leaves of *I. parviflorum*. (B) Longitudinal section of sieve tube elements of secondary vein (Sec) of a mature leaf showing sieve plate connections (arrowheads). (C) Sieve tube element of fourth order vein (Four) in mature leaf showing sieve plates (arrowheads) along lateral walls. (D) Relationship between sieve tube element length (blue circles) and radius (red triangles) in major veins of seedlings. (E) Longitudinal section of secondary vein of leaf from seedlings with sieve plate connection (arrowheads) between contiguous tubes. (A, D) Bars display standard error (SE); MID, midrib; PET, petiole; SEC, secondary vein; TERC, terciary vein. Scale bars: 500 μm.

framework with our data, and even though future works will likely elucidate whether this pattern is consistent across woody plants, our results point to a critical spatiotemporal regulation of sieve tube number and size in stems.

Phloem scaling in leaf veins of *I. parviflorum*

Unlike in the stems, mature leaves of *Illicium parviflorum* show a similar number of vascular elements of both xylem and the phloem, a 1:1 relationship that appears to be conserved across vein orders. These results are consistent with the idea of a physiological dependence between xylem and phloem (Zwieniecki et al., 2004; Sevanto et al., 2011; Hölttä et al., 2013). Indeed, the proportion of sieve tubes in the petioles of herbaceous species varies substantially, from the roughly 30% of sieve tubes in *Beta vulgaris* (Geiger et al., 1969), to 17% and 23% of *Cucurbita* species and potato, respectively (Crafts, 1931, 1933). While having a higher proportion of sieve tubes in the petioles has consequences for mass transfer from the leaves to the stems, the 1:1 relationship between the phloem and the xylem in the leaves of *I. parviflorum* implies that the increasing total conductive area of the xylem and phloem in the major veins results from a higher number of conduits toward the petiole, similar to the described reduction in phloem conduit number in the single-veined needles of pines (Ronellenfitsch et al., 2015). In addition, different vein hierarchies in the leaves of *I. parviflorum* have a scaling relationship of sieve tubes that is similar to what was recently reported for the reticulate-veined leaves of poplar (Carvalho et al., 2017a) and dichotomously veined *Ginkgo* (Carvalho et al., 2017b). However, the sieve tube elements are shorter (and slightly thinner) at the petiole in *Illicium parviflorum* leaves than within the major leaf veins.

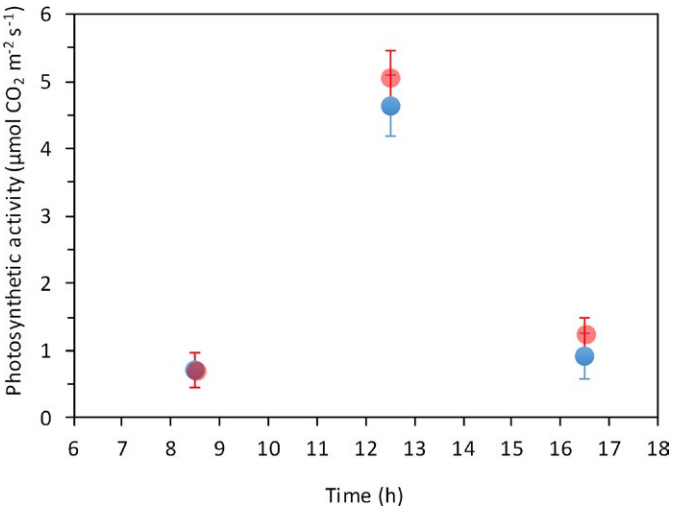

FIGURE 6. Photosynthetic activity in *Illicium parviflorum*. Comparison between assimilation rates of adult plants (blue, lower symbols) and seedlings (red, upper symbols) in the same greenhouse conditions at three times during the day. Error bars (SE) emphasize overlapping averages between both plant types.

Shorter sieve tubes in the phloem of the petiole may have implications for the regulation of pressure within the sieve tubes in leaves, especially at the times of maximum turgidity (i.e., maximum sugar export rates). We observed a higher number of sieve areas in the plates connecting the sieve tubes in the petiole; thus, this feature may attenuate at least in part a putative pressure increase (Carvalho et al., 2018). It would be desirable to obtain pore size in the sieve tubes of different vein orders and therefore check whether it concords with the hydraulic models for energy conservation, such as da Vinci's rule or Murray's law (Murray, 1926; Richter, 1980; McCulloh et al., 2003). Nevertheless, the role of the petiole in regulating sugar export from leaves has not been extensively explored across angiosperms and requires further attention (Grimm et al., 1997; Ray and Jones, 2018).

The directional flow in the sieve tubes of the major veins in *Illicium* leaves contrasts with the anatomy of the sieve tubes in the minor veins, which have numerous sieve areas pervading their lateral walls. The massive presence of sieve areas in the lateral walls of sieve tube elements from minor veins is in line with the idea of a division of function between the minor veins, which mainly work as sugar loaders, and major veins, where directional transport occurs within leaves (Russin and Evert, 1985; Turgeon, 2006; Carvalho et al., 2017a, 2018). A high number of symplasmic connections typically associate with passive sugar loading in the minor veins (van Bel et al., 1992; Turgeon, 1996; Gamalei et al., 2000; Rennie and Turgeon, 2009; Turgeon, 2010; Davidson et al., 2011; Zhang et al., 2014), but the heterogeneity of the species evaluated leave this question still unresolved (Slewinski et al., 2013). So far, sugar radiolabeling appears as the most reliable measure of loading type, which has yet to be applied to *Illicium parviflorum* leaves. As a member of the ANA grade of flowering plants, of which a majority are adapted to shaded environments, *Illicium* could likely fit with the previously hypothesized passive sugar loading in woody angiosperms of the understory (Gamalei, 1989, 1991). However, this feature appears to be labile among the extant members of the ANA grade, such as the sister lineage of all angiosperms *Amborella*, reported to be an active loader (Turgeon and Medville, 2011; Comtet et al., 2017).

Developmental flexibility and carbon limitation at the sources in the understory

Our estimations of the turgor pressures required to drive sap transport in *I. parviflorum* are within the range of osmotic values for phloem sap reported for a wide range of species (Jensen et al., 2013). These measurements thus support the validity of the Münch hypothesis (Münch, 1930) as the mechanism of sugar transport in understory shrubs, consistent with models of phloem transport in both angiosperm and gymnosperm trees (Thompson and Holbrook, 2003; De Schepper et al., 2013; Jyske and Holtta, 2015; Liesche et al., 2015; Comtet et al., 2017). However, our calculations indicate that

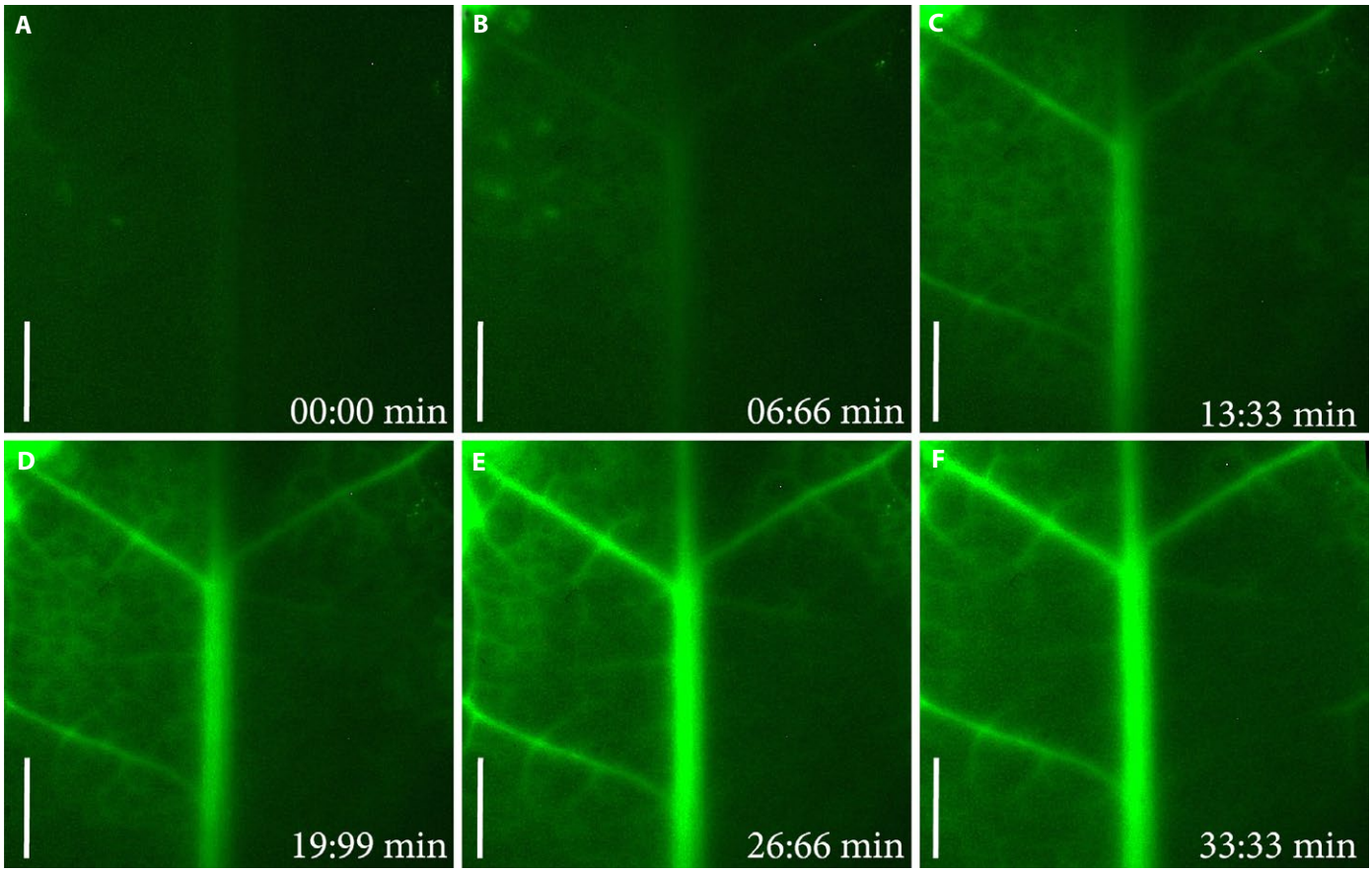

FIGURE 7. Velocity of sap within phloem of *Illicium parviflorum*. Time-lapse images of leaf from seedling showing advancement of carboxyfluorescein dye through phloem. Scale bars = 1000 µm.

even without increases in stem diameter, *I. parviflorum* branches could reach significant lengths without compromising phloem transport.

In addition, our evaluations of carbon low assimilation rates in greenhouse conditions are consistent with the low in situ measurements previously reported in the field (Feild et al., 2003a, b, 2004, 2009). Interestingly, the size of sieve tube elements, both diameter and length, in the major veins of the leaves of seedlings are approximately three times larger than in mature leaves. In parallel, the measured velocity of sap in the seedlings is 3-fold higher than in adult leaves, suggesting a functional flexibility of the phloem through ontogeny. Faster transport rates through the phloem of saplings would imply more efficient transport of sugars during rapid sun flecks, which account for one third of the total photosynthesis in the tropical understory (Pearcy, 1987). However, faster transport rates could reflect lower storage of carbohydrates in the leaves in response to sink strength for example, compared to the slower rates in adult plants. Phloem velocity in seedlings and adult plants has only been evaluated in one herbaceous species (Savage et al., 2013), and phloem sap velocity was variable in seedlings depending on the bundle and developmental stage. Phloem velocity is important from the perspective of sink strength because the faster transport of carbohydrates in the seedlings implies typically faster growth rates. However, whether this developmental dynamic is consistent across flowering plants requires further investigations.

CONCLUSIONS

Despite the understory origins of woody angiosperms, organismal scaling of sieve tube elements of the phloem appears as a conserved mechanism that predates the origin of woody flowering plants, and likely seed plants in general (see Woodruff et al., 2004; Liesche et al., 2015; Liesche, 2017). Angiosperm colonization of the vertical niche implied a number of structural innovations that led to a higher functional efficiency and thus productivity (Koch et al., 2004; Savage et al., 2017; Gleason et al., 2018). However, our knowledge on phloem functioning in the extant lineages of the basal angiosperm grade is still in its infancy. For the first time, we here evaluated in detail phloem anatomy and physiology in a member of the Austrobaileyales clade and offered a developmental angle that may help to explain the plasticity of the phloem in the light-limited environments where these lineages likely evolved. With respect to the phloem of adult plants, the major structural difference between the sieve tubes of *I. parviflorum* and those found in angiosperm trees is their much smaller sieve plate pores. Such a slight difference suggests that evolutionary changes in sieve tube structure could have critically influenced the structure and functioning of forest ecosystems.

Extant angiosperm taxa composing the component clades of the ANA grade (i.e., *Amborella*, Nymphaeales, Austrobaileyales, which are successive sister groups to all other flowering plants) consist of no more than 220 species. Yet, the spectrum of their life forms range from aquatic herbaceous (the whole Nymphaeales clade), to

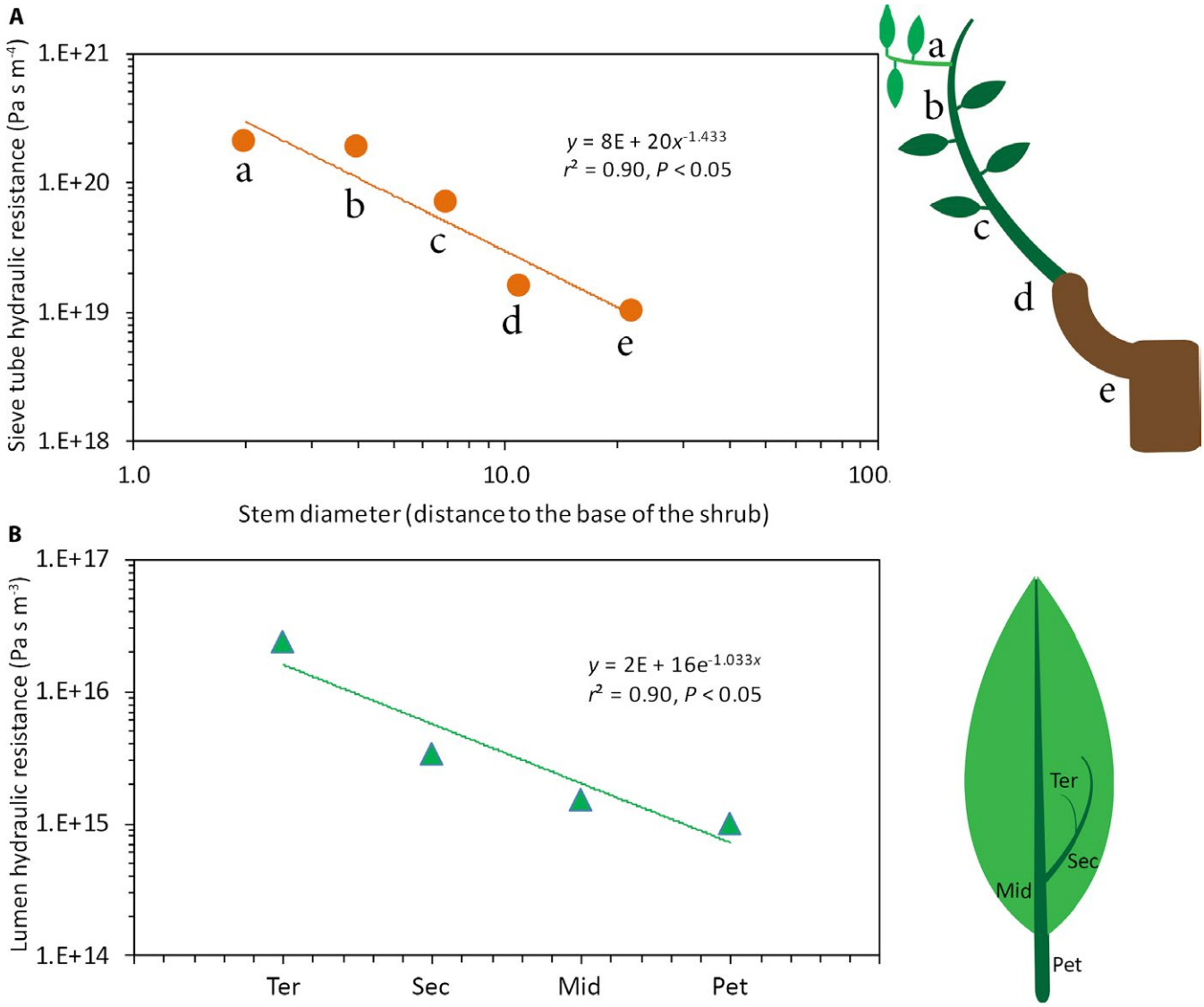

FIGURE 8. Sieve tube hydraulic resistance in aerial parts of *Illicium parviflorum*. (A) Inverse relationship between sieve element resistances per length at each stem diameter (related with distance to base of stem). (B) Sieve tube lumen resistance in major veins of mature leaves of *Illicium parviflorum*.

shrubs and lianas of the tropical understory in both the monotypic Amborellales and the Austrobaileyales. From a physiological angle, the evolution of physiological performance during angiosperm radiation has typically been inferred from the perspective of a single organ, such as leaves (Brodribb and Feild, 2010) or vascular traits of the xylem in mature plants (Feild and Arens, 2005, 2007). However, broader reconstruction of ancestral ecophysiological traits further requires organismal and developmental approaches, especially taking into account understudied tissues, such as the phloem. Knowing the parameters that condition sap flow through the phloem is particularly relevant in plants that acquired arborescent forms, since their size requires efficient internal transport tissues and they play an outsize role in structuring forest ecosystems. We propose that developmental and organismal heterogeneity of sieve tube elements across extant member of the basal angiosperm grade (see Behnke, 1986) are key elements for the reconstruction of traits that compose different strata in ancestral and contemporary forests. Thus, suites of functional vascular traits including perforation plates of the xylem (Feild and Wilson, 2012) and sieve plates of the phloem, may have been selected during early angiosperm evolution, allowing woody flowering plants to extend beyond their understory origins.

ACKNOWLEDGEMENTS

This work was funded by the National Science Foundation IOS 1456845 research grant to N.M.H. We are grateful to William E. (Ned) Friedman for kindly sharing plant material and lab facilities and to the staff of the Arnold Arboretum of Harvard University for continuous support. We thank Yongjiang Zhang for help with LI-COR measurements, Jessica Gersony and Kasia Zieminska for thoughtful feedback on the manuscript, and Nuria Blanco-Moure for help with edits. The authors also acknowledge the reviewers' comments, which greatly improved the manuscript.

DATA ACCESSIBILITY

Data archives are available in the digital public repository Harvard Data Verse at https://dataverse.harvard.edu/dataset.xhtml?persistentId=doi:10.7910/DVN/EMF8FC.

SUPPORTING INFORMATION

Additional Supporting Information may be found online in the supporting information tab for this article.

APPENDIX S1. Phloem in stems and leaves of *Illicium parviflorum*.

APPENDIX S2. Cross-sectional area of the vascular tissues along three areas of the major veins of mature leaves in *Illicium parviflorum*: petiole, midrib and tip of major vein.

APPENDIX S3. Linear correlations between the total number of phloem and xylem cells per vascular area between ray parenchyma in mature leaves.

APPENDIX S4. Linear correlations between total number of phloem and cambial cells and between phloem and xylem cells per vascular area between ray parenchyma in seedlings.

LITERATURE CITED

Bailey, I. W., and C. G. Nast. 1948. Morphology and relationships of *Illicium*, *Schisandra* and *Kadsura*: I. Stem and leaf. *Journal of the Arnold Arboretum* 29: 77–89.

Barral, A., B. Gomez, T. S. Feild, C. Coiffard, and V. Daviero-Gomez. 2013. Leaf architecture and ecophysiology of an early basal eudicot from the Early Cretaceous of Spain. *Botanical Journal of the Linnean Society* 173: 594–605.

Behnke, H. 1986. Sieve element characters and the systematic position of *Austrobaileya*, Austrobaileyaceae—with comments to the distinction and definition of sieve cells and sieve-tube members. *Plant Systematics and Evolution* 152: 101–121.

Boyce, C. K., and J. E. Lee. 2017. Plant evolution and climate over geological timescales. *Annual Review of Earth and Planetary Sciences* 45: 61–87.

Brodribb, T. J., and T. S. Field. 2010. Leaf hydraulic evolution led a surge in leaf photosynthetic capacity during early angiosperm diversification. *Ecology Letters* 13: 175–183.

Canny, M. J. 1973. Phloem translocation. University Press, Cambridge, UK.

Carlquist, S. 1982. Wood anatomy of *Illicium* (Illiciaceae): phylogenetic, ecological, and functional interpretations. *American Journal of Botany* 60: 1587–1598.

Carlquist, S., and E. L. Schneider. 2002. Vessels of *Illicium* (Illiciaceae): range of pit membrane remnant presence in perforations and other vessel details. *International Journal of Plant Sciences* 163: 755–763.

Carpenter, K. J. 2005. Stomatal architecture and evolution in basal angiosperms. *American Journal of Botany* 92: 1595–1615.

Carvalho, M. R., R. Turgeon, T. Owens, and K. J. Niklas. 2017a. The hydraulic architecture of *Ginkgo* leaves. *American Journal of Botany* 104: 1285–1298.

Carvalho, M. R., R. Turgeon, T. Owens, and K. J. Niklas. 2017b. The scaling of the hydraulic architecture in poplar leaves. *New Phytologist* 214: 145–157.

Carvalho, M. R., J. M. Losada, and K. J. Niklas. 2018. Phloem networks in leaves. *Current Opinion in Plant Biology* 43: 29–35.

Coiffard, C., B. Gómez, J. Kva4ček, and F. Thévenard. 2006. Early angiosperm ecology: evidence from the Albian-Cenomanian of Europe. *Annals of Botany* 98: 495–502.

Comtet, J., R. Turgeon, and A. D. Stroock. 2017. Phloem loading through plasmodesmata: a biophysical analysis. *Plant Physiology* 175: 904–915.

Crafts, A. S. 1931. Movement of organic materials in plants. *Plant Physiology* 6: 1–41.

Crafts, A. S. 1933. Sieve-tube structure and translocation in the potato. *Plant Physiology* 8: 81–104.

Davidson, A., F. Keller, and R. Turgeon. 2011. Phloem loading, plant growth form, and climate. *Protoplasma* 248: 153–163.

De Schepper, V., T. De Swaef, I. Bauweraerts, and K. Steppe. 2013. Phloem transport: a review of mechanisms and controls. *Journal of Experimental Botany* 64: 4839–4850.

Díaz-Espejo, A., and V. Hernández-Santana. 2017. The phloem–xylem consortium: until death do them part. *Tree Physiology* 37: 847–850.

Esau, K., V. I. Cheadle, and E. B. Risley. 1962. Development of sieve-plate pores. *Botanical Gazette* 123: 233–243.

Etxeberría, E., P. González, A. F. Borges, and C. Brodersen. 2016. The use of laser light to enhance the uptake of foliar-applied substances into citrus (*Citrus sinensis*) leaves. *Applications in Plant Sciences* 4: 1500106.

Feild, T. S., and N. C. Arens. 2005. Form, function and environments of the early angiosperms: merging extant phylogeny and ecophysiology with fossils. *New Phytologist* 166: 383–408.

Feild, T. S., and N. C. Arens. 2007. The ecophysiology of early angiosperms. *Plant, Cell & Environment* 30: 291–309.

Feild, T. S., and J. P. Wilson. 2012. Evolutionary voyage of angiosperm vessel structure–function and its significance for early angiosperm success. *International Journal of Plant Sciences* 173: 596–609.

Feild, T. S., N. C. Arens, and T. E. Dawson. 2003a. The ancestral ecology of angiosperms: emerging perspectives from extant basal lineages. *International Journal of Plant Sciences* 164: 129–142.

Feild, T. S., P. J. Franks, and T. L. Sage. 2003b. Ecophysiological shade adaptation in the basal angiosperm, *Austrobaileya scandens* (Austrobaileyaceae). *International Journal of Plant Sciences* 164: 313–324.

Feild, T. S., N. C. Arens, J. A. Doyle, T. E. Dawson, and M. J. Donoghue. 2004. Dark and disturbed: a new image of early angiosperm ecology. *Paleobiology* 30: 82–107.

Feild, T. S., D. S. Chatelet, and T. J. Brodribb. 2009. Ancestral xerophobia: a hypothesis on the whole plant ecophysiology of early angiosperms. *Geobiology* 7: 237–264.

Gamalei, Y. 1989. Structure and function of leaf minor veins in trees and herbs. *Trees* 3: 96–110.

Gamalei, Y. 1991. Phloem loading and its development related to plant evolution from trees to herbs. *Trees* 5: 50–64.

Gamalei, Y. V., M. V. Pakhomova, A. V. Syutkina, and O. V. Voitsekhovskaja. 2000. Compartmentation of assimilate fluxes in leaves. *Plant Biology* 2: 98–106.

Geiger, D. R., M. A. Saunders, and D. A. Cataldo. 1969. Translocation and accumulation of translocate in the sugar beet petiole. *Plant Physiology* 44: 1657–1665.

Ghouse, A. K. M., and A. Jamal. 1979. Sieve-tube proportion in the secondary phloem of some *Cassia* species. *Bulletin de la Société Botanique de France. Lettres Botaniques* 126: 207–211.

Ghouse, A. K. M., M. I. H. Khan, and S. Khan. 1976. Amount of sieve elements in the secondary phloem of some Myrtaceae. *Flora* 165: 489–492.

Gleason, S. M., M. Westoby, S. Jansen, B. Choat, U. G. Hacke, R. B. Pratt, R. Bhaskar, et al. 2016. Weak tradeoff between xylem safety and xylem-specific hydraulic efficiency across the world's woody plant species. *New Phytologist* 209: 123–136.

Gleason, S. M., A. E. Stephens, W. C. Tozer, C. J. Blackman, D. W. Butler, Y. Chang, A. M. Cook, et al. 2018. Shoot growth of woody trees and shrubs is predicted by maximum plant height and associated traits. *Functional Ecology* 32: 247–259.

Grimm, E., S. Jahnke, and K. Rothe. 1997. Photoassimilate translocation in the petiole of *Cyclamen* and *Primula* is independent of lateral retrieval. *Journal of Experimental Botany* 48: 1087–1094.

Hickey, L. J., and J. A. Doyle. 1977. Early Cretaceous fossil evidence for angiosperm evolution. *Botanical Review* 43: 3–104.

Hölttä, T., T. Vesala, S. Sevanto, M. Perämäki, and E. Nikinmaa. 2006. Modeling xylem and phloem water flows in trees according to cohesion theory and Münch hypothesis. *Trees* 20: 67–78.

Hölttä, T., M. Mencuccini, and E. Nikinmaa. 2009. Linking phloem function to structure: analysis with a coupled xylem–phloem transport model. *Journal of Theoretical Biology* 259: 325–337.

Hölttä, T., M. Kurppa, and E. Nikinmaa. 2013. Scaling of xylem and phloem transport capacity and resource usage with tree size. *Frontiers in Plant Science* 4: 496.

Jensen, K. H., J. Lee, T. Bohr, H. Bruus, N. M. Holbrook, and M. A. Zwieniecki. 2011. Optimality of the Münch mechanism for translocation of sugars in plants. *Journal of the Royal Society Interface* 8: 1155–1165.

Jensen, K. H., J. Liesche, T. Bohr, and A. Schulz. 2012a. Universality of phloem transport in seed plants. *Plant, Cell & Environment* 35: 1065–1076.

Jensen, K. H., D. L. Mullendore, N. M. Holbrook, T. Bohr, M. Knoblauch, and H. Bruus. 2012b. Modeling the hydrodynamics of phloem sieve plates. *Frontiers in Plant Science* 3: 151.

Jensen, K. H., J. A. Savage, and N. M. Holbrook. 2013. Optimal concentration for sugar transport in plants. *Journal of the Royal Society Interface* 10: 20130055.

Jensen, K. H., A. X. Valente, and H. A. Stone. 2014. Flow rate through microfilters: influence of the pore size distribution, hydrodynamic interactions, wall slip, and inertia. *Physics of Fluids* 26: 052004.

Jyske, T., and T. Hölttä. 2015. Comparison of phloem and xylem hydraulic architecture in *Picea abies* stems. *New Phytologist* 205: 102–115.

Khan, M. A., A. Kalimulla, and Z. Ahmad. 1992. Area occupied by sieve elements in the secondary phloem of some leguminous forest trees of Madhya Pradesh, India. *Flora* 186: 311–315.

Knoblauch, M., and W. S. Peters. 2017. What actually is the Münch hypothesis? A short history of assimilate transport by mass flow. *Journal of Integrative Plant Biology* 59: 292–310.

Knoblauch, M., M. Vendrell, E. de Leau, A. Paterlini, K. Knox, T. Ross-Elliot, A. Reinders, et al. 2015. Multispectral phloem-mobile probes: properties and applications. *Plant Physiology* 167: 1211–1220.

Knoblauch, M., J. Knoblauch, D. L. Mullendore, J. A. Savage, B. A. Babst, S. D. Beecher, A. C. Dodgen, et al. 2016. Testing the Münch hypothesis of long distance phloem transport in plants. *Elife* 5: e15341.

Koch, G. W., S. C. Sillett, G. M. Jennings, and S. D. Davis. 2004. The limits to tree height. *Nature* 428: 851–854.

Lawton, J. R. S., and M. J. Canny. 1970. The proportion of sieve elements in the phloem of some tropical trees. *Planta* 95: 351–354.

Liesche, J. 2017. Sucrose transporters and plasmodesmal regulation in passive phloem loading. *Journal of Integrative Plant Biology* 59: 311–321.

Liesche, J., H. J. Martens, and A. Schulz. 2011. Symplasmic transport and phloem loading in gymnosperm leaves. *Protoplasma* 248: 181–190.

Liesche, J., C. Windt, T. Bohr, A. Schulz, and K.H. Jensen. 2015. Slower phloem transport in gymnosperm trees can be attributed to higher sieve element resistance. *Tree Physiology* 35: 376–386.

Liesche, J., M. R. Pace, Q. Xu, Y. Li, and S. Chen. 2017. Height-related scaling of phloem anatomy and the evolution of sieve element end wall types in woody plants. *New Phytologist* 214: 245–256.

Linskens, H. F., and K. L. Esser. 1957. Über eine spezifische anfärbung der pollenschläuche im griffel und die zahl der kallosepfropfen nach selbstungund fremdung. *Naturwissenschaften* 44: 16–16.

Mathews, S., and M. J. Donoghue. 1999. The root of angiosperm phylogeny inferred from duplicate phytochrome genes. *Science* 286: 947–950.

McCulloh, K. A., J. S. Sperry, and F. R. Adler. 2003. Water transport in plants obeys Murray's law. *Nature* 421: 939–942.

Mullendore, D. L., C. W. Windt, H. Van As, and M. Knoblauch. 2010. Sieve tube geometry in relation to phloem flow. *Plant Cell* 22: 579–593.

Münch, E. 1930. Die stroffbewegungen in der pflanze. G. Fischer, Jena, Germany.

Murray, C. D. 1926. The physiological principle of minimum work. I. The vascular system and the cost of blood volume. *Proceedings of the National Academy of Sciences, USA* 12: 207–214.

Nikinmaa, E., T. Hölttä, P. Hari, P. Kolari, A. Mäkelä, S. Sevanto, and T. Vesala. 2013. Assimilate transport in phloem sets conditions for leaf gas exchange. *Plant, Cell & Environment* 36: 655–669.

Olson, M. E., D. Soriano, J. A. Rosell, T. Anfodillo, M. J. Donoghue, E. J. Edwards, C. León-Gómez, et al. 2018. Plant height and hydraulic vulnerability to drought and cold. *Proceedings of the National Academy of Sciences, USA* 115: 7551–7556.

Pace, M. R., L. G. Lohmann, and V. Angyalossy. 2011. Evolution of disparity between the regular and variant phloem in Bignonieae (Bignoniaceae). *American Journal of Botany* 98: 602–618.

Pace, M. R., S. Alcantara, L. G. Lohmann, and V. Angyalossy. 2015. Secondary phloem diversity and evolution in Bignonieae (Bignoniaceae). *Annals of Botany* 116: 333–358.

Parkinson, C. L., K. L. Adams, and J. D. Palmer. 1999. Multigene analyses identify the three earliest lineages of extant flowering plants. *Current Biology* 9: 1485–1491.

Pearcy, R. W. 1987. Photosynthetic gas exchange responses of Australian tropical forest trees in canopy, gap and understory micro-environments. *Functional Ecology* 1: 169–178.

Petit, G., and A. Crivellaro. 2014. Comparative axial widening of phloem and xylem conduits in small woody plants. *Trees* 28: 915–921.

Pickard, W. F. 2012. Münch without tears: a steady-state Münch-like model of phloem so simplified that it requires only algebra to predict the speed of translocation. *Functional Plant Biology* 39: 531–537.

Qiu, Y. L., J. Lee, F. Bernasconi-Quadroni, D. E. Soltis, P. S. Soltis, M. Zanis, E. A. Zimmer, et al. 2000. Phylogeny of basal angiosperms: analyses of five genes from three genomes. *International Journal of Plant Sciences* 161: 3–27.

Ray, D. M., and C. S. Jones. 2018. Scaling relationships and vessel packing in petioles. *American Journal of Botany* 105: 667–676.

Rennie, E. A., and R. Turgeon. 2009. A comprehensive picture of phloem loading strategies. *Proceedings of the National Academy of Sciences, USA* 106: 14162–14167.

Richter, I. A. 1980. The notebooks of Leonardo da Vinci. University Press, Oxford, UK.

Rockwell, F. E., J. T. Gersony, and N. M. Holbrook. 2018. Where does Münch flow begin? Sucrose transport in the pre-phloem pathway. *Current Opinion in Plant Biology* 43: 101–107.

Ronellenfitsch, H., J. Liesche, K. H. Jensen, N. M. Holbrook, A. Schulz, and E. Katifori. 2015. Scaling of phloem structure and optimality of photoassimilate transport in conifer needles. *Proceedings of the Royal Society, B, Biological Sciences* 282: 20141863.

Russin, W. A., and R. F. Evert. 1985. Studies on the leaf of *Populus deltoides* (Salicaceae): ultrastructure, plasmodesmatal frequency, and solute concentrations. *American Journal of Botany* 72: 1232–1247.

Savage, J. A., M. A. Zwieniecki, and N. M. Holbrook. 2013. Phloem transport velocity varies over time and among vascular bundles during early cucumber seedling development. *Plant Physiology* 163: 1409–1418.

Savage, J. A., M. J. Clearwater, D. F. Haines, T. Klein, M. Mencuccini, S. Sevanto, R. Turgeon, and C. Zhang. 2016. Allocation, stress tolerance and carbon transport in plants: How does phloem physiology affect plant ecology? *Plant, Cell & Environment* 39: 709–725.

Savage, J. A., S. Beecher, L. Clerx, J. T. Gersony, J. Knoblauch, J. M. Losada, K. H. Jensen, et al. 2017. Maintenance of carbohydrate transport in tall trees. *Nature Plants* 3: 965.

Seleznyova, A. N., and J. Hanan. 2018. Mechanistic modelling of coupled phloem/xylem transport for L-systems: combining analytical and computational methods. *Annals of Botany* 121: 991–1003.

Sevanto, S., T. Hölttä, and N. M. Holbrook. 2011. Effects of the hydraulic coupling between xylem and phloem on diurnal phloem diameter variation. *Plant, Cell & Environment* 34: 690–703.

Slewinski, T. L., C. Zhang, and R. Turgeon. 2013. Structural and functional heterogeneity in phloem loading and transport. *Frontiers in Plant Science* 4: 244.

Soltis, P. S., D. E. Soltis, and M. W. Chase. 1999. Angiosperm phylogeny inferred from multiple genes as a tool for comparative biology. *Nature* 402: 402–404.

Soltis, D., P. Soltis, P. Endress, M. W. Chase, S. Manchester, W. Judd, L. Majure, and E. Mavrodiev. 2018. Phylogeny and evolution of the angiosperms: revised and updated edition. University Press, Chicago, IL, USA.

Thompson, M. V., and N. M. Holbrook. 2003. Application of a single-solute nonsteady-state phloem model to the study of long-distance assimilate transport. *Journal of Theoretical Biology* 220: 419–455.

Turgeon, R. 1996. Phloem loading and plasmodesmata. *Trends in Plant Science* 1: 418–423.

Turgeon, R. 2006. Phloem loading: how leaves gain their independence. *BioScience* 56: 15–24.

Turgeon, R. 2010. The puzzle of phloem pressure. *Plant Physiology* 154: 578–581.

Turgeon, R., and R. Medville. 2011. *Amborella trichopoda*, plasmodesmata, and the evolution of phloem loading. *Protoplasma* 248: 173–180.

Upchurch, G., D. Dilcher, and W. Crepet. 1984. Cuticle evolution in Early Cretaceous angiosperms from the Potomac Group of Virginia and Maryland. *Annals of the Missouri Botanical Garden* 71: 522–550.

van Bel, A. J., Y. V. Gamalei, A. Ammerlaan, and L. P. Bik. 1992. Dissimilar phloem loading in leaves with symplasmic or apoplasmic minor-vein configurations. *Planta* 186: 518–525.

Woodruff, D. R., B. J. Bond, and F. C. Meinzer. 2004. Does turgor limit growth in tall trees? *Plant, Cell & Environment* 27: 229–236.

Woodruff, D. R., F. C. Meinzer, and K. A. McCulloh. 2016. Forest canopy hydraulics. *In* K. Hikosaka, K. Niinemets, Ü. Anten, and P. R. Niels [eds.], Canopy photosynthesis: from basics to applications, 187–217. Springer, Dordrecht, Netherlands.

Zhang, C., L. Han, T. L. Slewinski, L. Thomas, J. Sun, J. Zhang, Z. Y. Wang, and R. Turgeon. 2014. Symplastic phloem loading in poplar. *Plant Physiology* 166: 306–313.

Zwieniecki, M. A., and C. K. Boyce. 2014. Evolution of a unique anatomical precision in angiosperm leaf venation lifts constraints on vascular plant ecology. *Proceedings of the Royal Society, B, Biological Sciences* 281: 20132829.

Zwieniecki, M. A., P. J. Melcher, T. S. Feild, and N. M. Holbrook. 2004. A potential role for xylem–phloem interactions in the hydraulic architecture of trees: effects of phloem girdling on xylem hydraulic conductance. *Tree Physiology* 24: 911–917.